# Local isotropy in distorted turbulent boundary layers at high Reynolds number

By Seyed G. Saddoughi

## 1. Motivation and background

This is a report on the continuation of our experimental investigations (Saddoughi 1993; Saddoughi & Veeravalli 1993) of the hypothesis of local isotropy in shear flows. This hypothesis, which states that at sufficiently high Reynolds numbers the small-scale structures of turbulent motions are independent of large-scale structures and mean deformations (Kolmogorov 1941), has been used in theoretical studies of turbulence and computational methods such as large-eddy simulation. Since Kolmogorov proposed his theory, there have been many experiments, conducted in wakes, jets, mixing layers, a tidal channel, and atmospheric and laboratory boundary layers, in which attempts have been made to verify – or refute – the local-isotropy hypothesis. However, a review of the literature over the last five decades indicated that, despite all these experiments in shear flows, there was no consensus in the scientific community regarding this hypothesis, and, therefore, it seemed worthwhile to undertake a fresh experimental investigation into this question.

### *1.1 Plane boundary layer*

In our previous reports, we presented hot-wire measurements of the velocity fluctuations in the test-section-ceiling boundary layer of the 80- by 120-foot Full-Scale Aerodynamics Facility at NASA Ames Research Center, the world's largest wind tunnel. At our measurement location, the boundary-layer thickness, $\delta$, was about 1.1 m, and the maximum Reynolds numbers based on momentum thickness, $R_\theta$, and on Taylor microscale, $R_\lambda$, were approximately 370,000 and 1,450 respectively. These were the largest ever attained in laboratory boundary-layer flows. The boundary layer developed over a rough surface, but the Reynolds-stress profiles agreed with canonical data sufficiently well for our purposes. Spectral and structure-function relations for isotropic turbulence were used to test the local-isotropy hypothesis, and our results established the condition under which local isotropy can be expected.

Here we use a Cartesian co-ordinate system $x_i = (x, y, z)$ with $x$-axis along the flow direction, $y$-axis normal to the solid surface, and $z$-axis in the spanwise direction. The respective mean-velocity components in these directions are $U_i = (U, V, W)$, and the fluctuating components are $u_i = (u, v, w)$. Overbars denote time averages.

Our plane boundary-layer data showed that, to within the accuracy of measurement, the shear-stress co-spectral density $E_{12}(k_1)$, which is the most sensitive indicator of local isotropy, fell to zero at a wavenumber about a decade *larger* than that at which the energy spectra first followed $-5/3$ power laws. At the highest Reynolds number, $E_{12}(k_1)$ vanished about one decade *before* the start of the dissipation range, and it remained zero in the dissipation range.

We found that the lower-wavenumber limit of locally-isotropic behavior of the shear-stress co-spectra is given by $k_1\sqrt{\varepsilon/S^3} \approx 10$ where $S$ is the mean shear, $\partial U/\partial y$, and $\varepsilon$ is the average turbulent energy dissipation rate per unit mass. Our investigation also indicated that for energy spectra this limit could be relaxed to $k_1\sqrt{\varepsilon/S^3} \approx 3$; this is Corrsin's (1958) criterion, with the numerical value obtained from our data. The existence of an isotropic inertial range requires that this wavenumber be much less than the wavenumber at the onset of viscous effects, $k_1\eta \ll 1$ ($\eta$ is the Kolmogorov length scale), so that the combined condition (Corrsin 1958 and Uberoi 1957) is $S\sqrt{\nu/\varepsilon} \ll 1$.

Among other detailed results, it was observed that in the dissipation range, the energy spectra had a simple exponential decay (Kraichnan 1959) with an exponent prefactor close to the value $\beta = 5.2$ obtained in direct numerical simulations at low Reynolds number. Plots of compensated spectra, $k^{5/3}, E(k_1)$, proved to be a very sensitive test in the inertial subrange. The Kolmogorov constants obtained from the one-dimensional data at high Reynolds numbers satisfied the isotropic relations for the spectra and the second-order structure functions, and the constant for the three-dimensional spectrum, $C$, was estimated to be $1.5 \pm 0.1$ (Monin & Yaglom 1975). Spectral "bumps" between the $-5/3$ inertial range and the dissipative range were observed on all the compensated energy spectra. The shear-stress co-spectra rolled-off with a $-7/3$ power law and scaled linearly with $S$ (Lumley 1967).

In summary, our results confirmed the local-isotropy hypothesis for "simple" shear layers, and it was shown that one decade of inertial subrange with truly negligible shear-stress co-spectral density requires $S\sqrt{\nu/\varepsilon}$ not more than about 0.01 (for a shear layer with turbulent kinetic energy production $\approx$ dissipation, this implies a microscale Reynolds number of about 1500).

### *1.2 Distorted boundary layer*

The effects of extra mean strain rates on the large-scale structure of shear flows (Bradshaw 1973) have been investigated extensively. The unanswered question for us was *"will our criteria for the existence of local isotropy hold for complex non-equilibrium flows"*. Therefore, experiments to address this question were designed for the 80- by 120-foot wind tunnel. One possible experiment was to study the plane-of-symmetry flow in front of an obstacle placed vertically in a fully-developed two-dimensional turbulent boundary layer, e.g. a circular cylinder placed with its axis perpendicular to the plate. There have been a number of experimental investigations dealing with the large-scale structural changes that occur in this kind of flow (Johnston 1960; Hornung & Joubert 1963; Belik 1973; Mehta 1984; Agui & Andreopoulos 1990; Devenport & Simpson 1990; to name a few). In this type of boundary layer, the pressure rises strongly as the obstacle is approached and in the plane of symmetry of the flow the boundary layer is also influenced by the effects of lateral divergence (Saddoughi & Joubert 1991). Hence, in addition to the basic shear, $\partial U/\partial y$, the extra strain rates involved in the flow are $\partial U/\partial x$, $\partial V/\partial y$ and

$\partial W/\partial z$. To obtain the desired effects, the size of the cylinder should be at least of the order of the thickness of the boundary layer. To conduct such an experiment in the 80′ by 120′ wind tunnel, a very large cylinder had to be fixed to the ceiling of the tunnel. This presented considerable construction difficulties. Here some of the results taken in front of this cylinder at the highest speed of the tunnel will be discussed.

## 2. Accomplishments

### *2.1 Apparatus and measurement techniques*

The only possible way for attaching an obstacle to the ceiling of the 80- by 120-foot wind tunnel was to use one of the existing light ports for this purpose. Since the diameter of our test cylinder had to be larger than the clear opening of a typical light port, we had to use two concentric cylinders. As shown in Plate 1(a), the main cylinder is a ready-made light-weight polyethylene tank (wall thickness = $\frac{1}{4}''$, diameter $D = 4'$ and height $L = 6'$) and the inner (second) cylinder is a $\frac{1}{2}''$ thick, 8″ diameter aluminum (6061-T651) tube, which extends for about 6′ into the attic through the light port. Steel rods are bolted to the aluminum cylinder. A $\frac{1}{4}''$ thick high-density polyethylene plate and a $\frac{1}{8}''$ thick aluminum plate are respectively bolted to the inside and outside of the bottom of the polyethylene tank. The effective wall thickness at the bottom of the tank is $\frac{5}{8}''$. Another $\frac{1}{4}''$ thick high-density polyethylene plate is bolted to the top of the tank, and the space between the aluminum cylinder and the tank is filled with high-density Polyurethane foam. This provided us with a fairly light-weight (500 lb) and solid cylinder.

From the attic above the test-section ceiling, this whole unit was pulled up through the light port and was attached to the attic structure. Plate 1(b) shows the test cylinder in place as viewed from inside the test section. The NASA safety requirements were satisfied, and the cylinder and its attachments were designed for maximum possible aerodynamic load and dynamic loading due to seismic activity with an overall factor of safety of 5 on yield strength.

Another light port upstream of the cylinder was used for traversing the probe through the boundary layer. Therefore, our measurement location was fixed at $x/D \approx 0.85$ with respect to the front of the cylinder. The measurement strategy, instrumentation, and procedure were all similar to those explained by Saddoughi (1993) and Saddoughi & Veeravalli (1993), and details will not be repeated here.

### *2.2 Results and discussion*

The measurements to be discussed here correspond to the maximum reference velocity of the tunnel, $U_{ref} = 51.25$ m/s. The normalized profiles of the longitudinal mean velocity, $U/U_{ref}$, for the present distorted boundary layer are compared with the profiles obtained for both the high-speed and low-speed cases of the plane boundary layer in figure 1, where $y$ is the distance from the wall. Also shown in this figure are the least-squares polynomial fit to each of the data sets (solid lines), which have been used to obtain the mean-flow integral parameters for each experiment. The shape of the velocity profile for the distorted boundary layer is typical

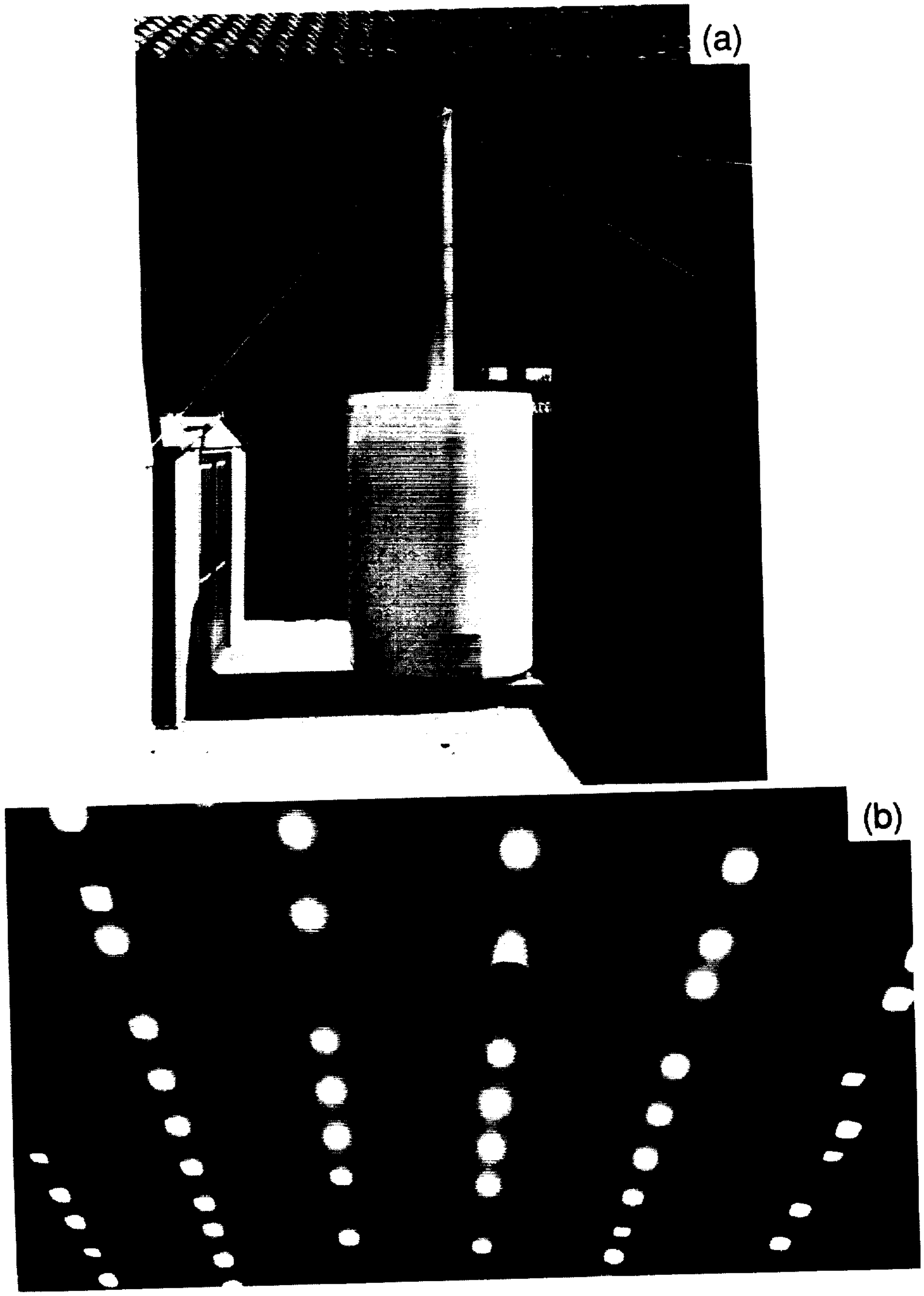


Plate 1. Test cylinder. (a) Outer (main) cylinder (polyethylene tank: wall thickness = $\frac{1}{4}''$, diameter $D = 4'$, and height $L = 6'$) and the inner (support) cylinder (aluminum 6061-T651 tube: $\frac{1}{2}''$ thick, 8″ diameter and 12′ height). (b) Test cylinder attached to the ceiling of the 80′ X 120′ wind tunnel, as viewed from inside the test section.

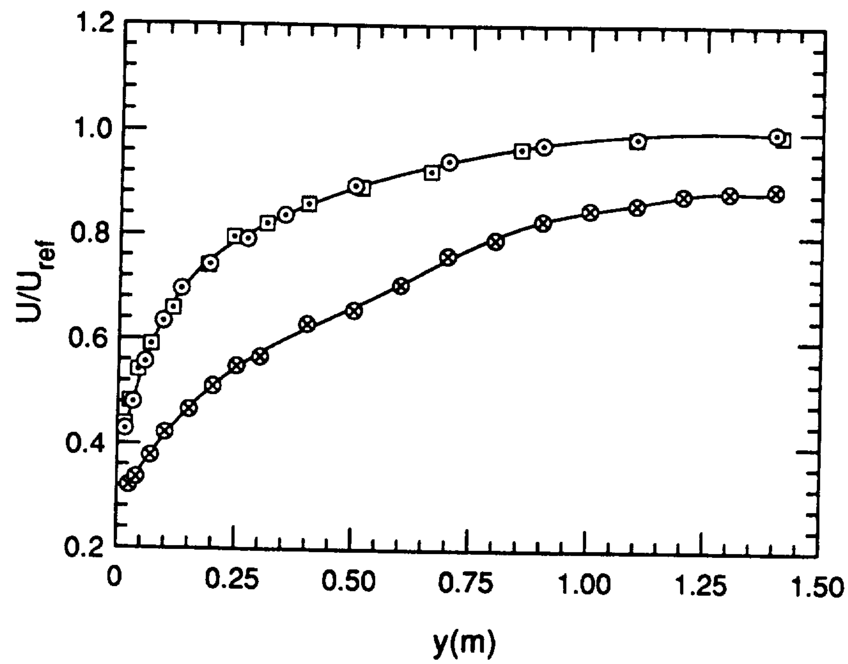


FIGURE 1. Normalized longitudinal mean-velocity profiles measured in plane and distorted boundary layers. ○ , $U_{ref} \approx 50$ m/s and □ , $U_{ref} \approx 10$ m/s plane boundary layer; ⊗ , $U_{ref} \approx 51$ m/s distorted boundary layer. The solid lines are the least-square polynomial fit to each data set.

of the adverse-pressure-gradient flows: reduction in $\partial U/\partial y$. The boundary-layer thickness, $\delta$ (the point where $U/U_e = 0.995$) has increased to approximately 1250 mm in the distorted boundary layer. Here the shape factor $H \approx 1.85$, and in the freestream the pressure coefficient $C_p \approx 0.23$.

Figure 2 shows the normalized profiles of the normal velocity component, $V/U_{ref}$, and the spanwise component, $W/U_{ref}$, which were measured by the X-wires in UV- and UW-mode respectively. It can be seen that, as expected, in the plane of symmetry of the flow the crossflow, $W$, is approximately equal to zero. A least-squares polynomial fit to the $V$ profile was used to obtain the values of $\partial V/\partial y$.

The magnitudes of the extra strain rate due to the streamline divergence, $\partial W/\partial z$, influencing the plane of symmetry of the flow can be obtained from $(\partial W/\partial z) = U(\partial \beta/\partial z)$ (see e.g. Saddoughi & Joubert 1991), where $\beta$ is the flow yaw angle measured at different spanwise locations $z$. The profiles of $\beta$ measured by a yaw-meter probe for three spanwise locations ($z/D = -0.21, 0, 0.21$) through the boundary layer are shown in figure 3. The profiles are typical of three-dimensional boundary layers: larger flow yaw angles near the wall than the freestream. Finally, the continuity equation was used to obtain the $\partial U/\partial x$ values.

The profiles of the Reynolds normal stresses $(\overline{u_1^2}/U_{ref}^2, \overline{u_2^2}/U_{ref}^2, \overline{u_3^2}/U_{ref}^2)$, and

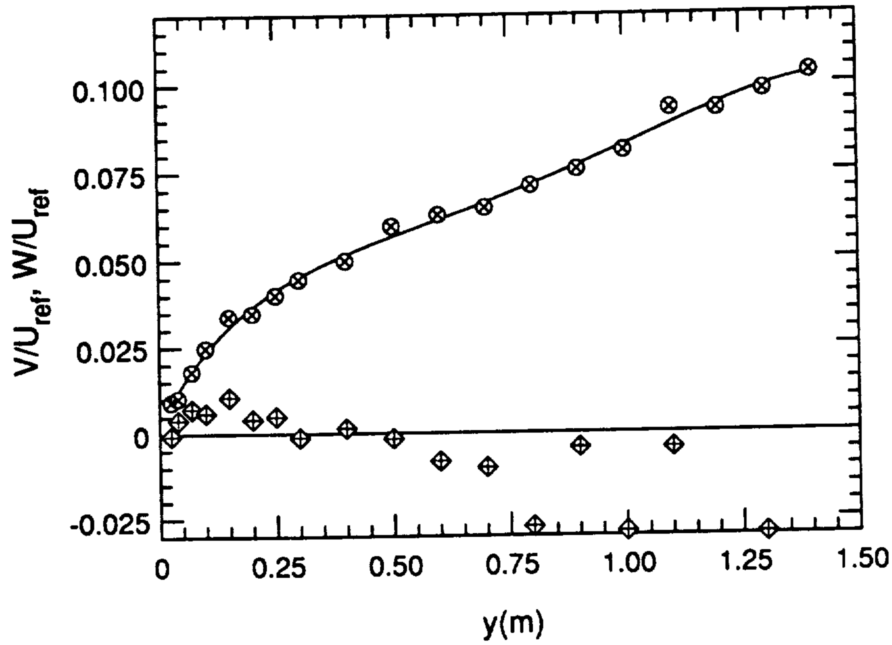


FIGURE 2. Normalized vertical and spanwise mean-velocity profiles measured in the plane of symmetry of the distorted boundary layer. ⊗, $V/U_{ref}$; ⟴, $W/U_{ref}$.

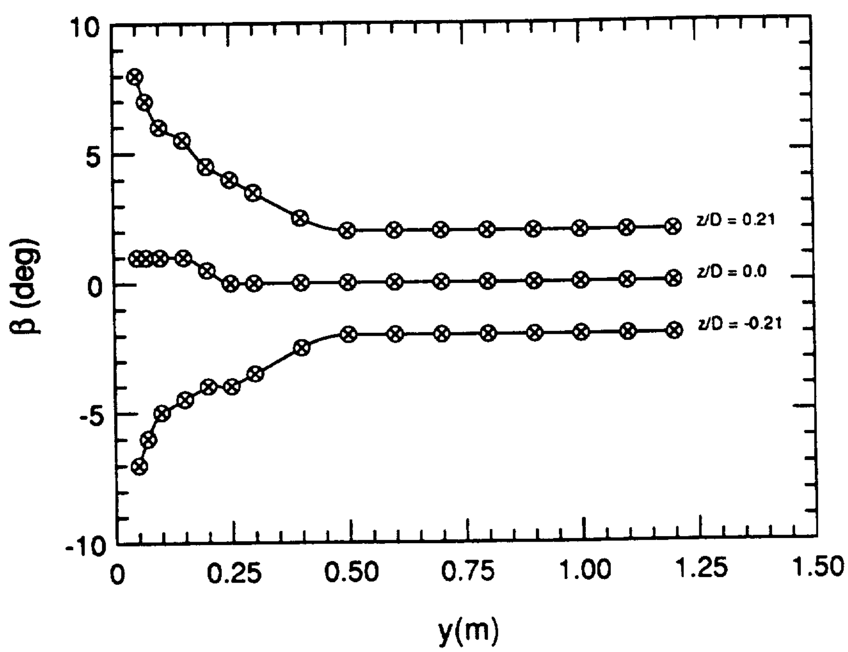


FIGURE 3. Flow yaw-angle profiles measured in the distorted boundary layer at different spanwise locations.

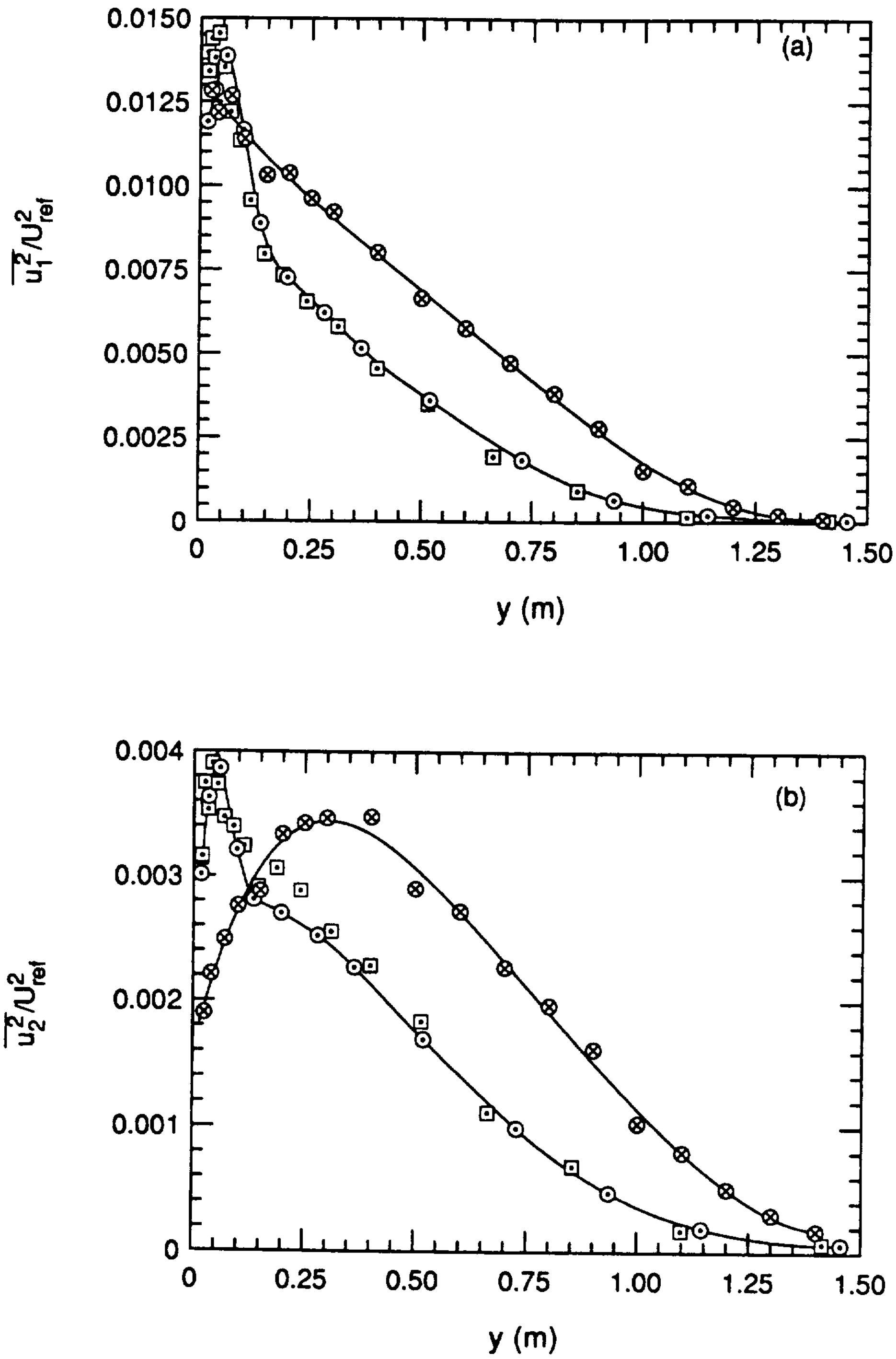


FIGURE 4(A,B). For caption see next page.

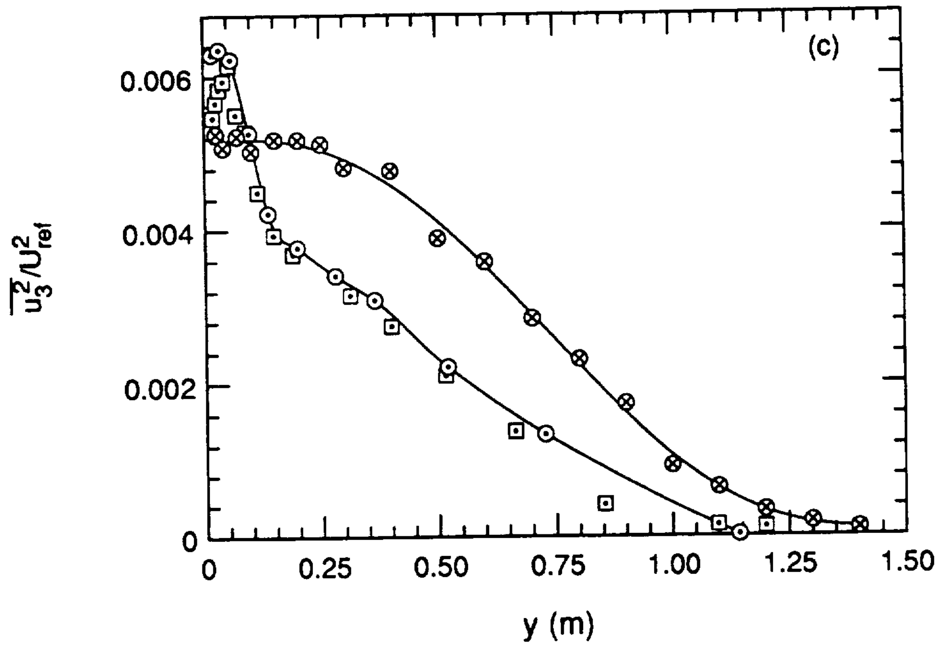


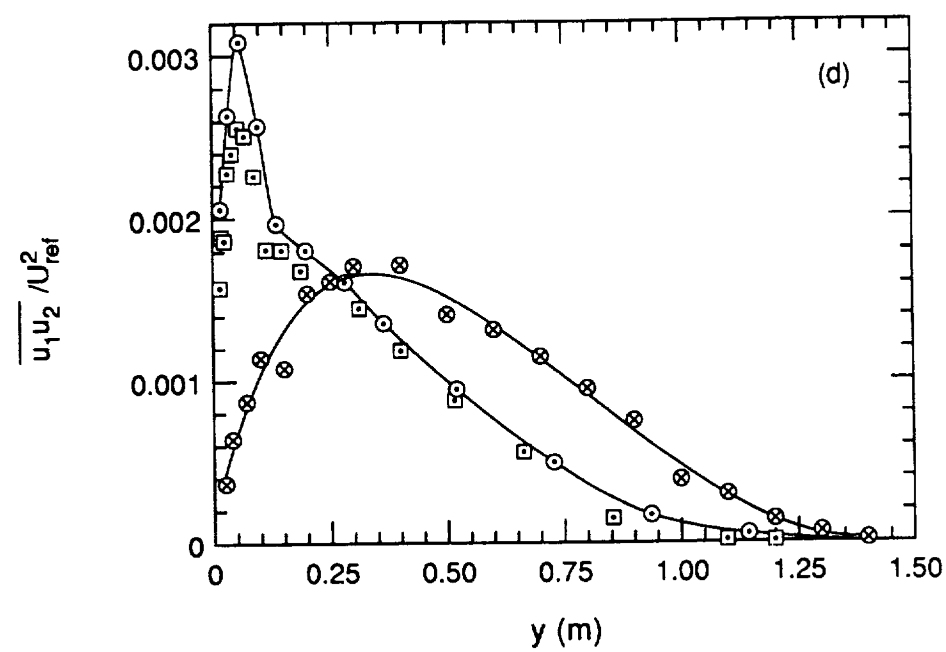


FIGURE 4. Profiles of Reynolds stresses measured in plane and distorted boundary layers: (a) $\overline{u_1^2}/U_{ref}{}^2$, (b) $\overline{u_2^2}/U_{ref}{}^2$, (c) $\overline{u_3^2}/U_{ref}{}^2$, (d) $\overline{u_1u_2}/U_{ref}{}^2$. For key to symbols see figure 1.

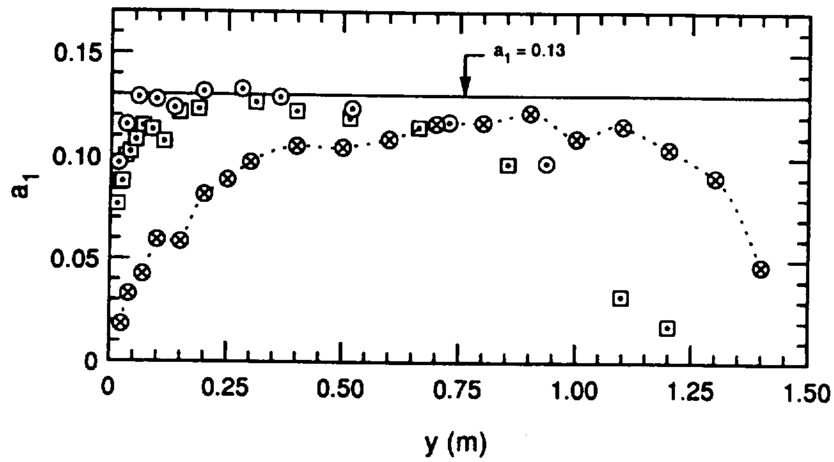


FIGURE 5. The structure parameter, $a_1 \equiv -\overline{u_1u_2}/q^2$. The solid line is the canonical smooth-wall value (Townsend 1976). For key to symbols see figure 1.

the shear stress, $-\overline{u_1u_2}/U^2_{ref}$, for the distorted and plane boundary layers are compared in figure 4. The profiles for the distorted boundary layer appear to be quite different from the plane flow case. The peaks of $\overline{u_2^2}$ and the shear stress, $-\overline{u_1u_2}$, profiles have moved away from the wall to $y \approx 300$ mm, and in the outer part of the layer the values of all the Reynolds stresses have increased. The changes in the large-scale structure of turbulence can be seen in figure 5, which shows the profiles of Townsend's structure parameter, $a_1 \equiv (-\overline{u_1u_2}/q^2)$, where $q^2$ $(\equiv \overline{u_iu_i})$ is twice the turbulent kinetic energy per unit mass. The large drop in the values of this parameter in the inner part of the boundary layer, and their recovery to the canonical values in the outer part of the layer are apparently due to the effects of adverse pressure gradients (see Bradshaw 1967).

The spectral measurements of the three components of the velocity made at $y$ = 100 mm, 300 mm, and 500 mm are analyzed here. The location $y$ = 300mm was chosen because, as shown earlier, the peak of the Reynolds stresses occurred at this position in the layer. For these three locations, the values of the extra-mean-strain rates, $(\partial U/\partial x)/(\partial U/\partial y)$, $(\partial V/\partial y)/(\partial U/\partial y)$, and $(\partial W/\partial z)/(\partial U/\partial y)$ are all larger than 0.1, which according to Bradshaw (1973) should produce large non-linear effects on the large-scale structures of the boundary layer.

In figure 6, we examine the $II(\equiv -\frac{1}{2}b_{ij}b_{ji})$ and $III(\equiv \frac{1}{3}b_{ij}b_{jk}b_{ki})$ invariants map of the Reynolds stress anisotropy tensor (Lumley & Newman 1977; Lee & Reynolds 1985), $b_{ij} \equiv (\overline{u_iu_j}/q^2) - \delta_{ij}/3$, where $\delta_{ij} = 1$ or 0 for $i = j$ or $i \neq j$ respectively. The data points shown in this figure correspond to those positions in both the boundary layers where spectral measurements were taken. It appears that for both the plane and distorted layers, the values are close to the axisymmetric expansion limit. However, note that there is a fairly large increase for the distorted boundary layer, particularly at $y$ = 100 mm, which is represented by the highest point in each

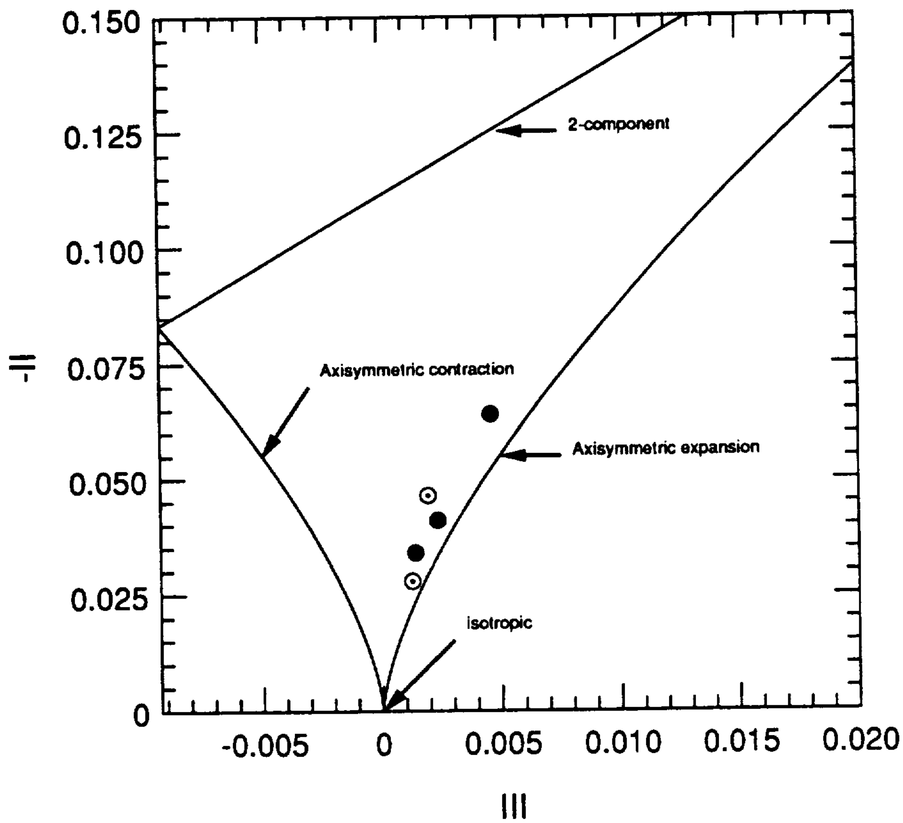


FIGURE 6. Anisotropy invariant map of Reynolds stress. Open and solid symbols are for the plane and distorted boundary layers respectively. The maximum value in each case corresponds to measurements at $y = 100$ mm.

data set.

As an example of the spectral measurements, figure 7 shows Kolmogorov's universal scaling of the one-dimensional longitudinal power spectra at the inner-layer position of the distorted boundary layer and the mid-layer position of the plane boundary layer, compared with a compilation of previous experimental work taken from Chapman (1979) with later additions. The Reynolds numbers for the present distorted boundary layer have increased substantially, and a maximum $R_\lambda \approx 1960$ has been obtained for the inner-layer position.

The intensity (or rapidity) of a mean strain rate can be measured in terms of $s = \sqrt{s_{ij}s_{ij}/2}$, (Lee & Reynolds 1985). To be consistent with our earlier definition, we shall use $S = 2s$ as the equivalent mean strain rate. To test the local-isotropy hypothesis in the distorted layer, log-linear plots of the correlation-coefficient spectra, $R_{12}(k_1) \equiv -E_{12}(k_1)/\sqrt{E_{11}(k_1)E_{22}(k_1)}$, are plotted versus the non-dimensional wavenumber $k_1\sqrt{\varepsilon/S^3}$ in figure 8. In isotropic flow the shear-stress co-spectrum, $E_{12}(k_1)$, which satisfies $\int_0^\infty E_{12}(k_1)\,dk_1 = -\overline{u_1u_2}$, is equal to zero. This indicates

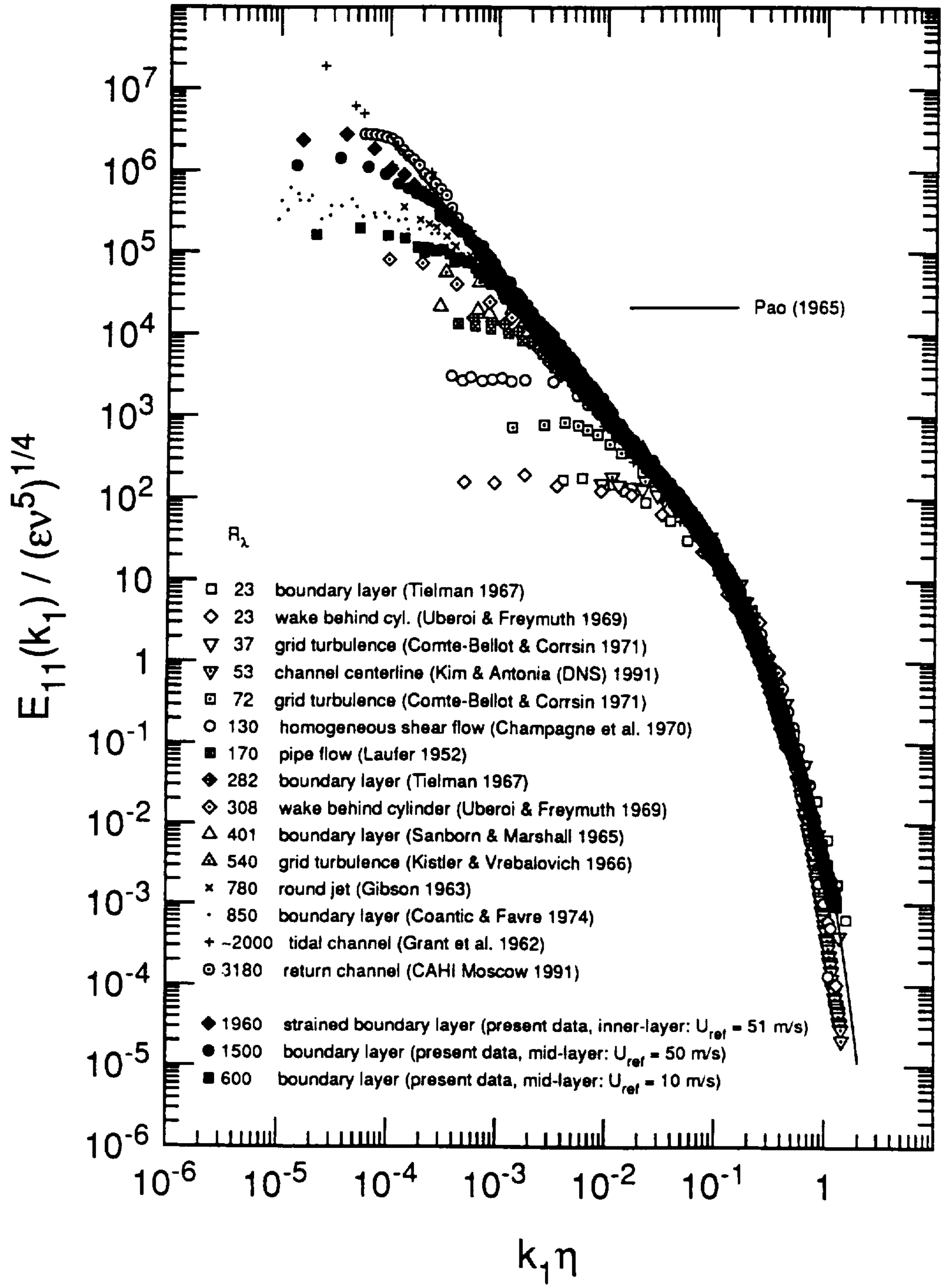


FIGURE 7. Kolmogorov's universal scaling for one-dimensional longitudinal power spectra. The present mid-layer and inner-layer spectra for the respective plane and distorted boundary layers are compared with data from other experiments. This compilation is from Chapman (1979), with later additions.

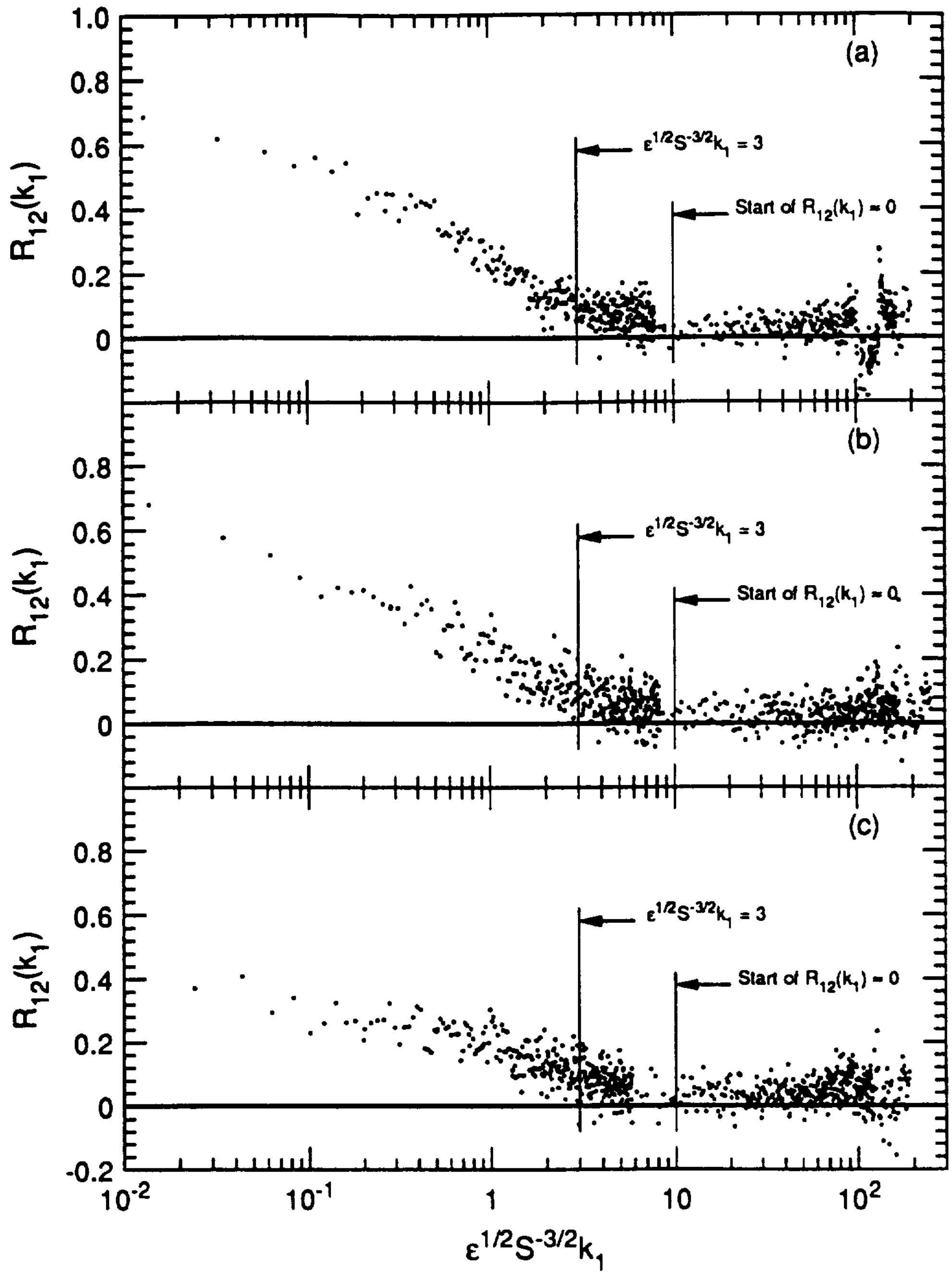


FIGURE 8. Correlation-coefficient spectra obtained at different locations in the distorted boundary layer for $U_{ref} = 51$ m/s: wavenumber scaled with $\sqrt{\varepsilon/S^3}$. (a) $y = 500$ mm, $R_\lambda \approx 1960$; (b) $y = 300$ mm, $R_\lambda \approx 1950$; (c) $y = 100$ mm, $R_\lambda \approx 1750$.

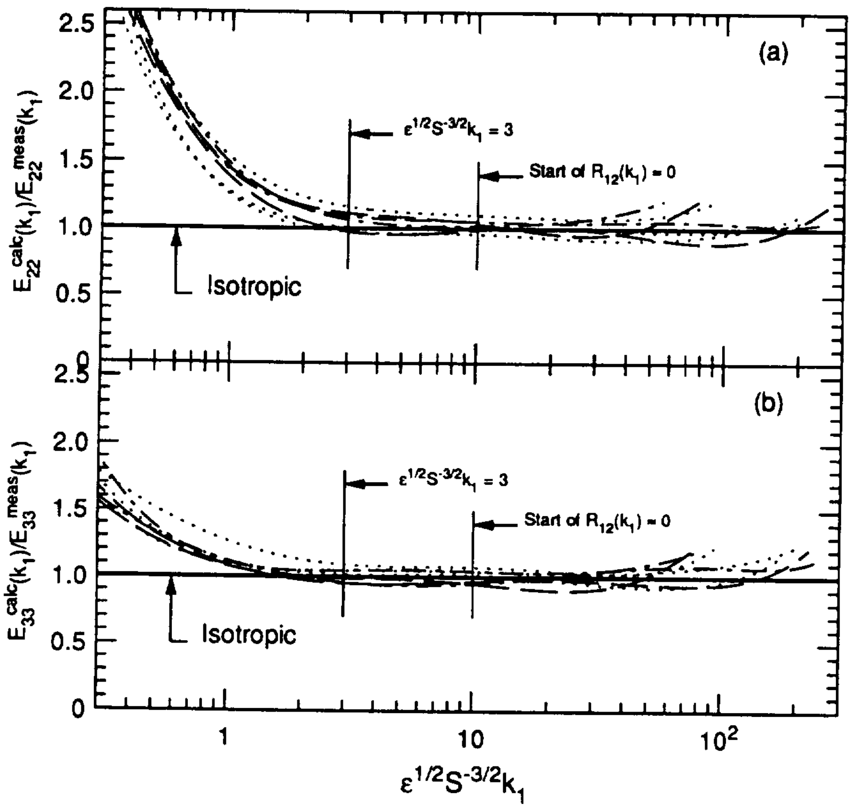


FIGURE 9. Ratios of calculated to measured transverse spectra at different locations and freestream velocities in the plane (- - - - ) and distorted (········ ) boundary layers: wavenumber scaled with $\sqrt{\varepsilon/S^3}$.

that for local isotropy the correlation-coefficient spectrum should fall to zero at high wavenumbers. For all the three measurement positions in the boundary, the Corrsin-Uberoi condition $S_c^* \equiv S\sqrt{\nu/\varepsilon} \ll 1$ was satisfied. It can seen from figure 8 that at all the measurement locations $R_{12}(k_1)$ reaches the isotropic value of zero at $k_1\sqrt{\varepsilon/S^3} \approx 10$, which is the same limit found for the plane boundary layer for the onset of local isotropy.

If the motion is isotropic, the transverse spectra $E_{22}(k_1)$ and $E_{33}(k_1)$ are uniquely determined by the longitudinal spectrum $E_{11}(k_1)$ (e.g. Batchelor 1953): $E_{22}(k_1) = E_{33}(k_1) = \frac{1}{2}(1 - k_1\frac{\partial}{\partial k_1})E_{11}(k_1)$. The transverse spectra, $E_{22}^{calc}(k_1)$ and $E_{33}^{calc}(k_1)$, can be calculated from the measured longitudinal spectrum, $E_{11}^{meas}(k_1)$, using the above equation. An anisotropy measure may be defined as $E_{\alpha\alpha}^{calc}(k_1)/E_{\alpha\alpha}^{meas}(k_1)$, where $\alpha = 2$ or 3 corresponds to $u_2$ or $u_3$ respectively. These anisotropy measures should be equal to 1.0 in an isotropic flow. We have used $9^{th}$-order, least-squares polynomial log-log fits to the data to calculate these measures, which are shown in figure 9 scaled using the length scale $\sqrt{\varepsilon/S^3}$. The data for the plane boundary layer are also shown in this figure. It is obvious that the uncertainty in estimating the $S$ values for the distorted boundary layer is larger than the plane case.

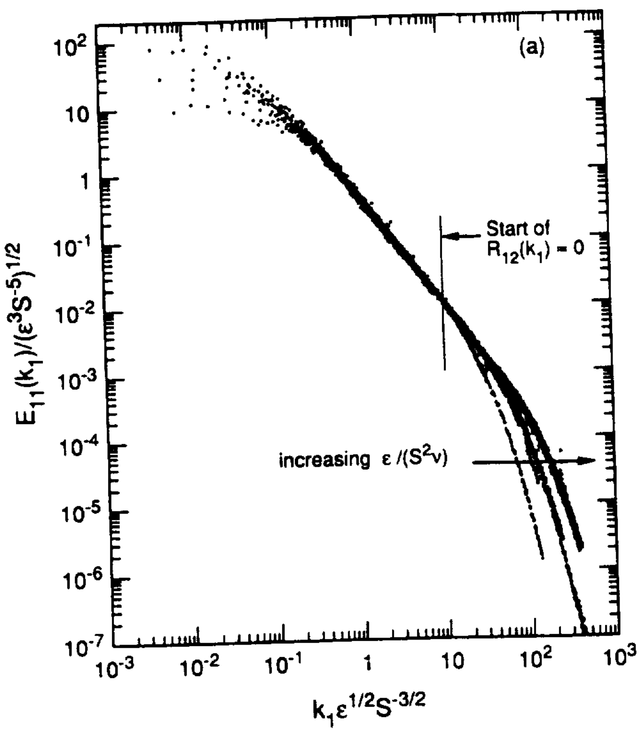


FIGURE 10(a). For caption see next page.

However, it appears that a reasonably good collapse is obtained and local isotropy of energy spectra is achieved ($\pm10\%$) in the inertial subrange for non-dimensional wavenumbers $k_1\sqrt{\varepsilon/S^3} > 3$.

For both plane and distorted boundary layers, the collapse of the longitudinal and transverse spectra achieved using $\sqrt{\varepsilon/S^3}$ and $\sqrt{\varepsilon/S}$ as length and velocity scales, respectively, is shown in figure 10. As to be expected, these scales will not collapse the low and high-wavenumber ranges of the spectra. Also marked on this figure is the wavenumber corresponding to the start of $R_{12}(k_1) \approx 0$, which is about one decade higher than the start of the $-5/3$ law on the energy spectra. This plot clearly demonstrates the fact that a $-5/3$ law does not necessarily imply local isotropy. We also note that in the *high-wavenumber* range the extent of the $-5/3$ law does not increase with $R_\lambda$, but it is a function of $(\varepsilon/S^2\nu)$, which is the Reynolds number based on the above length and velocity scales. However, the accuracy of this observation will be examined further after completing the upcoming low-speed measurements.

## Acknowledgements

We wish to thank Dr. Fredric Schmitz, Chief of the Full-Scale Aerodynamics Research Division at NASA Ames for permitting us to use their facility and to

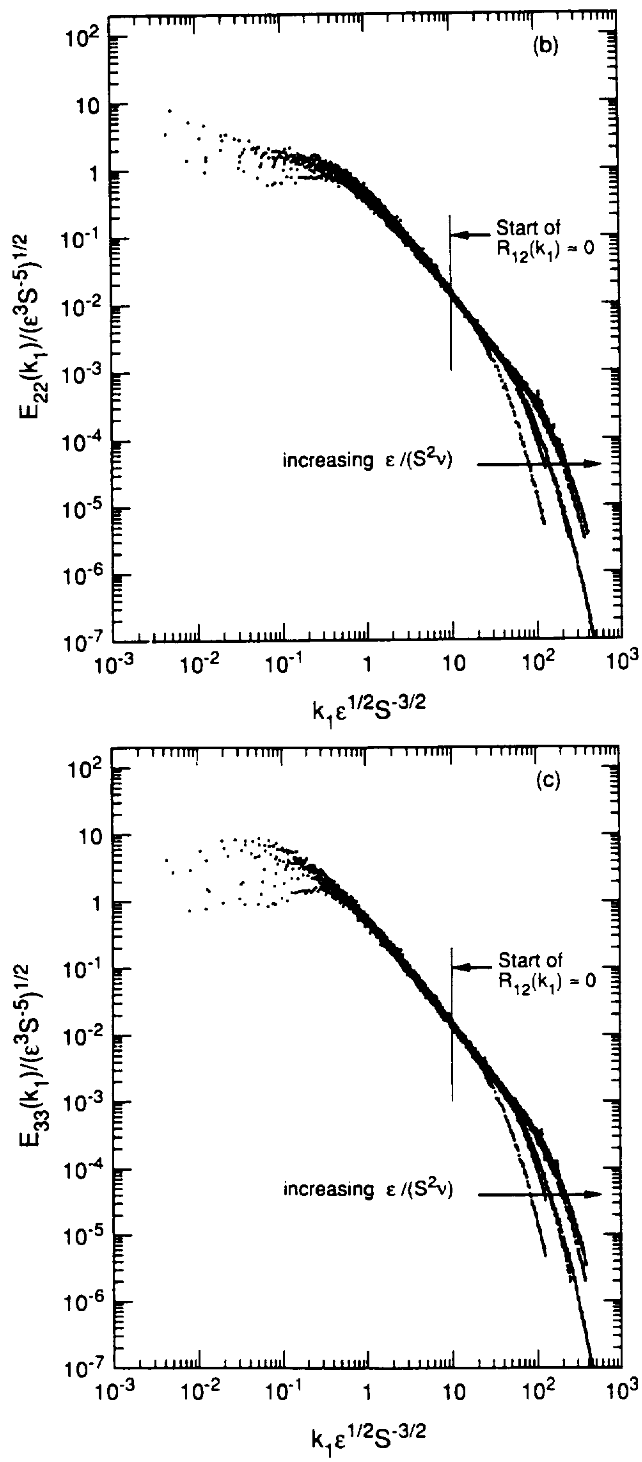


FIGURE 10. Spectra measured at different locations and freestream velocities in the plane and distorted boundary layers non-dimensionalized using $\sqrt{\varepsilon/S^3}$ and $\sqrt{\varepsilon/S}$ as length and velocity scales respectively. (a) $E_{11}(k_1)$; (b) $E_{22}(k_1)$; (c) $E_{33}(k_1)$.

thank Dr. James Ross, Group Leader–Basic Experiments, who has been and will be in charge of coordinating our tests in the 80′ by 120′ wind tunnel. We also wish to thank Ms. Wendy Lanser, Mr. Gavin Botha, Mr. Ken Kono and Mr. Bill Dotty. Our experiments would have not been possible without their help and efforts.

During the design and construction of the cylinder and its accessories, we received extensive advice from Prof. Bill Reynolds and Mr. Robin Birch of Stanford University and Dr. Joseph Huang of CALSPAN Corp. We gratefully thank them for all their suggestions. We wish to thank Prof. Bill Reynolds, Prof. Parviz Moin, Prof. Peter Bradshaw, and Dr. Bob Rogallo for many valuable discussions of our results. We have benefited from the expert advice of Prof. Roger Simpson. I am grateful to my wife, Elizabeth, and Mr. Eric Buice, who helped me with the measurements during all those "graveyard" shifts.

## REFERENCES

AGUI, J. & ANDREOPOULOS, J. 1990 Experimental investigation of a three-dimensional boundary layer flow in the vicinity of an upright wall mounted cylinder. *AIAA 90-1545.*

BATCHELOR, G. K. 1953 *The Theory of Homogeneous Turbulence.* Cambridge University Press.

BELIK, L. 1973 The secondary flow about circular cylinders mounted normal to a flat plate. *Aero Q.* **24**, 47-54.

BRADSHAW, P. 1973 Effects of streamline curvature on turbulent flow. *AGARDograph.* **169.**

BRADSHAW, P. 1967 The turbulence structure of equilibrium boundary layers. *J. Fluid Mech.* **29**, 625-645.

CHAPMAN, D. 1979 Computational aerodynamics development and outlook. *AIAA J.* **17**, 1293.

CORRSIN, S. 1958 On local isotropy in turbulent shear flow. *Report NACA R & M 58B11.*

DEVENPORT, W. J. & SIMPSON, R. L. 1990 Time-dependent and time-averaged turbulence structure near the nose of a wing-body junction. *J. Fluid Mech.* **210**, 23-55.

HORNUNG, H. G. & JOUBERT, P. N. 1963 The mean velocity profile in three-dimensional turbulent boundary layers. *J. Fluid Mech.* **15**, 368-384.

JOHNSTON, J. P. 1960 The turbulent boundary layer at a plane of symmetry in a three-dimensional flow. *Trans. A.S.M.E. Series D.* **82**, 622-628.

KOLMOGOROV, A. N. 1941 The local structure of turbulence in incompressible viscous fluid for very large Reynolds numbers. *C. R. Acad. Sci. U.R.S.S.* **30**, 301.

KRAICHNAN, R. H. 1959 The structure of isotropic turbulence at very high Reynolds numbers. *J. Fluid Mech.* **5**, 497.

LEE, M. J. & REYNOLDS, W. C. 1985 Numerical experiments on the structure of homogeneous turbulence. *Technical Report TF-24*. Department of Mechanical Engineering, Stanford University.

LUMLEY, J. L. 1967 Similarity and the turbulent energy spectrum. *Phys. Fluids.* **10,** 855-858.

LUMLEY, J. L. & NEWMAN, G. R. 1977 The return to isotropy of homogeneous turbulence. *J. Fluid Mech.* **82,** 161-178.

MEHTA, R. D. 1984 Effect of wing nose shape on the flow in a wing/body junction. *Aeronaut. J.* **88,** 456-460.

MONIN, A. S. & YAGLOM, A. M. 1975 *Statistical Fluid Mechanics,* vol. 2. M.I.T. Press.

SADDOUGHI, S. G. 1993 Local isotropy in high Reynolds number turbulent shear flows. *Annual Research Briefs-1992*, Center for Turbulence Research, Stanford University/NASA Ames. 237-262.

SADDOUGHI, S. G. & JOUBERT, P. N. 1991 Lateral straining of turbulent boundary layers. Part 1. Streamline divergence. *J. Fluid Mech.* **229,** 173-204.

SADDOUGHI, S. G. & VEERAVALLI, S. V. 1993 Local isotropy in turbulent boundary layers at high Reynolds number. *J. Fluid Mech.* To be published.

TOWNSEND, A. A. 1976 *The Structure of Turbulent Shear Flow, 2nd edn. Cambridge University Press.*

UBEROI, M. S. 1957 Equipartition of energy and local isotropy in turbulent flows. *J. Appl. Phys.* **28,** 1165-1170.